SC22 SciViz

Visualising an Immediate Giant-Impact Origin for the Moon

Jacob A. Kegerreis[1,2]*, Vincent R. Eke[1], Richard J. Massey[1], Sergio Ruiz-Bonilla[1], Thomas D. Sandnes[1], Luís F. A. Teodoro[3,4].

[1]Physics Department, Institute for Computational Cosmology, Durham University, UK. [2]NASA Ames Research Center, USA. [3]BAERI / NASA Ames Research Center, USA. [4]School of Physics and Astronomy, University of Glasgow, UK. *jacob.kegerreis@durham.ac.uk

Abstract

The Moon is typically thought to have slowly coalesced from debris ejected by a giant impact onto the early Earth. However, models of this idea struggle to explain the similar isotopic compositions of the Earth and Moon at the same time as their angular momenta, and the details of potential collision scenarios are hotly debated. We present visualisations of high-resolution simulations that reveal how giant impacts can immediately place Moon-like satellites into orbit far outside the Earth's disruption Roche limit. Even satellites that first pass within the limit can survive by being partially stripped and launched onto wider, stable orbits. This opens up new options for the Moon's early evolution and offers a simpler, single-stage scenario for the origin of the Moon. The animations provide a dramatic 3D perspective of these violent impact events that are traditionally visualised with only 2D projections, while remaining directly driven by the simulation data.

1 Introduction

The origin of the Moon is one of the most significant unsolved problems in planetary science. We present[1] 3D renders of two high-resolution simulations of giant impacts to examine an alternative possibility for the Moon's formation.

This SciViz submission is probably best categorised as an explanatory one, although we also find these visualisations are equally valuable for ourselves and other experts to inspect and gain intuition about these collisions and simulations in new ways.

In the canonical hypothesis for the Moon-forming impact, the early Earth is hit by a Mars-sized impactor, 'Theia' (Hartmann and Davis, 1975; Cameron and Ward, 1976; Canup et al., 2021). The collision ejects a debris disk that can explain the Moon's large mass, angular momentum, and tiny iron core; but it creates a Moon derived mostly from impactor material (Canup and Asphaug, 2001; Canup et al., 2021). This is a concern because the Moon has a near-identical isotopic composition to the Earth for many elements (Melosh, 2014; Meier et al., 2014; Lock et al., 2020), and it seems unlikely, though perhaps possible, that the impactor would already match the proto-Earth target's composition (Dauphas, 2017; Mastrobuono-Battisti and Perets, 2017; Schiller et al., 2018; Johansen et al., 2021).

Alternative impact scenarios have been proposed to improve on canonical models. High angular momentum impacts into rapidly spinning targets (Ćuk and Stewart, 2012; Lock et al., 2018) can eject and mix more proto-Earth material, as can a very large impactor (Canup, 2012). The excess angular momentum might be removable in or near the evection resonance, but removing the correct amount may be difficult (Rufu and Canup, 2020). Hit-and-run impacts can also make somewhat more target-rich disks (Reufer et al., 2012). Multiple impacts could create successive intermediate satellites that combine to form the Moon (Rufu et al., 2017), depending on the merger efficiency (Citron et al., 2018). Somewhat separately, a proto-Earth magma ocean could be more readily injected into orbit (Hosono et al., 2019), and numerical effects might be inhibiting mixing in simulations (Deng et al., 2019b). The circumstances required for some of these events may also have low likelihoods, though with only one Moon to study we are reminded that its origin could be improbable (Melosh, 2014).

Numerical simulations of giant impacts commonly use smoothed particle hydrodynamics (SPH)

[1] astro.dur.ac.uk/∼cklv53/sc22_sci_viz_kegerreis.mp4

to model planets using particles that evolve under gravity and pressure (Lucy, 1977; Gingold and Monaghan, 1977). Most previous Moon-formation simulations have used around 10^5–10^6 particles, but these resolutions can fail to converge on even large-scale outcomes of giant impacts, such as the planet's rotation period or the mass of ejected debris (Genda et al., 2015; Hosono et al., 2017; Kegerreis et al., 2019). Here we use up to 10^8 particles. At this resolution, each particle has a mass of 6×10^{16} kg and an effective size in the planet of ∼14 km. A lunar-mass satellite itself is then composed of around 10^6 particles, which enables us to inspect its composition in detail.

Directly produced satellites were found in some early simulations of giant impacts (Benz et al., 1987; Canup and Asphaug, 2001), but have typically been dismissed in terms of lunar formation (Canup and Asphaug, 2001; Asphaug, 2014) because of (1) then-justified low-resolution numerical concerns; (2) a lack of iron and of proto-Earth material; (3) overly fine-tuned requirements for the impact parameters; (4) and/or orbits that crossed interior to the Roche limit. In contrast, with orders of magnitude more particles, we find that stable satellites are produced (1) reliably at high numerical resolutions of at least 10^7 SPH particles; (2) with a Moon-like mass of iron and significant proto-Earth material; (3) over a small but appreciable range of impact angles and speeds especially for spinning planets (Ruiz-Bonilla et al., 2021); (4) and that satellites with Roche-interior initial trajectories often survive partial disruption to be torqued onto wider final orbits.

For this project, we used the Houdini VFX software and Redshift renderer to create 3D visualisations of Moon-forming SPH simulation data. We summarise the impact simulations in §2, and the content of and results behind the visualisations in §3, followed by a description of the rendering process. A brief discussion of the scientific implications and the visualisation outcomes are then given in §4.

2 SPH Simulations

The impact simulations were run using our open-source hydrodynamics and gravity code SWIFT[2], using a 'vanilla' form of SPH plus the Balsara (1995) switch for the artificial viscosity (Kegerreis et al., 2019), to a simulation time of 90 ks (25 hours), in a cubic box of side 120 $R_\oplus$. Any particles that leave the box are removed from the simulation.

The SWIFT code can function as a drop-in replacement for Gadget-2, which has been widely used for cosmological and planetary impact simulations (e.g. Springel, 2005; Ćuk and Stewart, 2012), but with a >30× faster runtime on representative cosmological problems (Borrow et al., 2018), and allows us to use ∼100–1000 times more particles than the typical standard for planetary simulations. This speed is partly a result of SWIFT's task-based approach to parallelism and domain decomposition (Gonnet, 2015). By evaluating and dividing up the work instead of just the data, this provides a dynamic way to achieve good load balancing across modern supercomputing architectures.

The proto-Earth target and Theia impactor are differentiated into an iron core and a rocky mantle containing 30% and 70% of the mass, respectively, with canonical-like masses of 0.877 and 0.133 $M_\oplus$. We use the updated ANEOS $Fe_{85}Si_{15}$ (Earth-core analogue) and forsterite equations of state (EoS) (Stewart et al., 2019), which encompass thermodynamically consistent models of multiple phases and improved fits to experimental data. The temperature at the surface is set to 2000 K, for a mantle specific entropy of 2.9 kJ K^{-1} kg^{-1}. The internal profiles are adiabatic with continuous temperature across the core–mantle boundary.

The planets' internal profiles are generated by integrating inwards while maintaining hydrostatic equilibrium[3], then the roughly equal-mass particles are placed to precisely match the resulting density profiles using the stretched equal-area method[4]. Before simulating the impact, a brief 10 ks settling simulation is first run for each body in isolation, to allow any final settling to occur. The specific entropies of the particles are kept fixed, enforcing that the particles relax themselves adiabatically.

3 Results and visualisations

3.1 Content

The first animation shows a simulation in which the satellite is immediately launched onto a wide and nearly circular orbit, as illustrated with a 2D projection by Fig. 1. We are also currently finalising a stand-alone version with captions.

Theia, the smaller body, collides with the Earth and ejects a large spray of debris from both planets, mostly rocky mantle plus some of the impactor's hot iron core. Most of this collects into two bodies: the inner remnant and outer satellite. The inner remnant then pulls the satellite forward, transferring angular momentum to slingshot the satellite

[2]SWIFT (Schaller et al., 2018) is publicly available at www.swiftsim.com.

[3]The WoMa code (Ruiz-Bonilla et al., 2021) for producing spherical and spinning planetary profiles and initial conditions is publicly available with documentation and examples at github.com/srbonilla/WoMa.

[4]SEAGen (Kegerreis et al., 2019) is publicly available at github.com/jkeger/seagen.

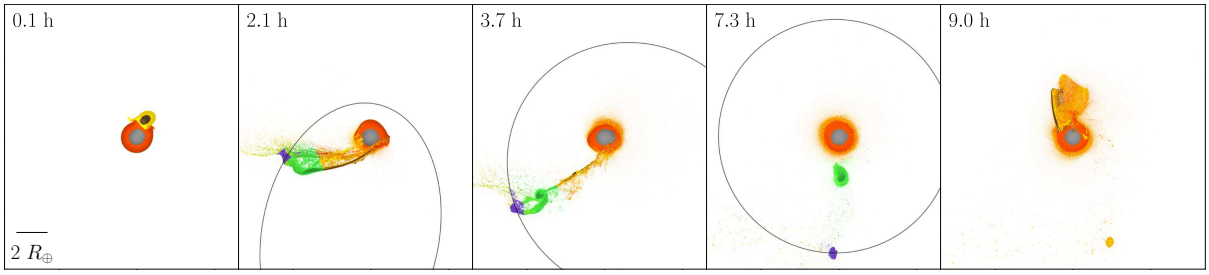

Figure 1: Illustrative snapshots from the first-animation simulation, where a satellite is placed directly onto a wide orbit. In the middle panels, the particles that will form the satellite and inner remnant are highlighted in purple and green. The black lines show the estimated orbit. Grey and orange show the proto-Earth's core and mantle material respectively, and brown and yellow the same for Theia. The colour luminosity varies slightly with the internal energy. The annotated time is measured from first contact, so the simulation began at −1 h.

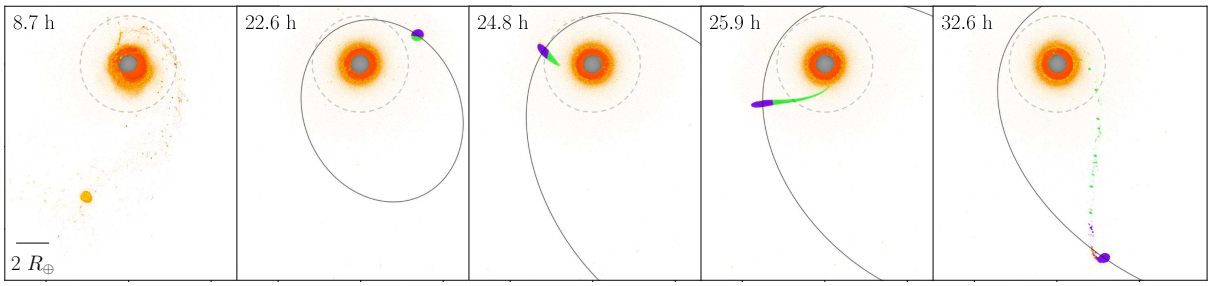

Figure 2: Illustrative snapshots from the second-animation simulation, of the first periapsis passage after the satellite-forming inital impact, where the satellite is partially stripped and torqued to end up on a stable final orbit. Colours and annotations are the same as in Fig. 1, except here purple and green highlight the material that will end up in the final satellite and that will be stripped from the initial body, respectively. The dashed line indicates the Roche limit.

into orbit, before falling back to re-impact the target.

The resulting satellite has a mass of 0.69 $M_☾$ and a nearly circular orbit with a periapsis of 7.1 $R_\oplus$, far outside the Roche limit of ∼2.9 $R_\oplus$ (inside of which it would be tidally disrupted) and even likely beyond the evection and eviction resonances for a moderate rotation period (Touma and Wisdom, 1998; Ćuk and Stewart, 2012).

The second animation shows a similar simulation of a collision with a different impact angle, where the satellite is then not launched out quite as far, and its initial periapsis falls within the Roche limit. However, not only does the satellite survive partial tidal disruption, but the stripped material transfers angular momentum to the surviving satellite and torques it onto a stable, Roche-exterior final orbit, as illustrated in 2D by Fig. 2. This significantly extends the parameter-space range of scenarios that can produce a Moon-like satellite.

We see the similar first stages of the impact from a more close-in viewpoint for the initial shock wave and recombining of the ejecta into the two bodies. Most of the bright core material falls back into the proto-Earth, followed by the inner remnant that in this case is mostly swallowed up compared with the grazing second impact of the first scenario.

The satellite then falls falls deep inside the Roche limit with an initial periapsis of 2.6 $R_\oplus$. The tidal forces tear off about one third of its mass, stripped out into a long tidal tail, for a final mass of 1.1 $M_☾$. The surviving satellite continues on a new, wider orbit with its periapsis now raised outside the Roche limit to 3.1 $R_\oplus$, protecting it from further disruption. We find that this is a reliable and predictable process across a variety of initial low periapsis and initial satellite masses.

3.2 Creation process

The visualisations were created using the Houdini procedural VFX program and rendered using Redshift. Our primary goal was not to create a fully physically accurate render of what the impact would truly have looked like – which would both be extremely complicated to model and would likely result in an immediately obscuring cloud of gas and debris. Instead, we aimed to render the data from the simulations directly enough to illustrate this scenario for the origin of the Moon and to convey the cataclysmic nature of these planet-reshaping collisions.

We use the SPH simulations to output 'snapshot' files of the particle positions, velocities, densities, and other properties every 100 s of simulation time.

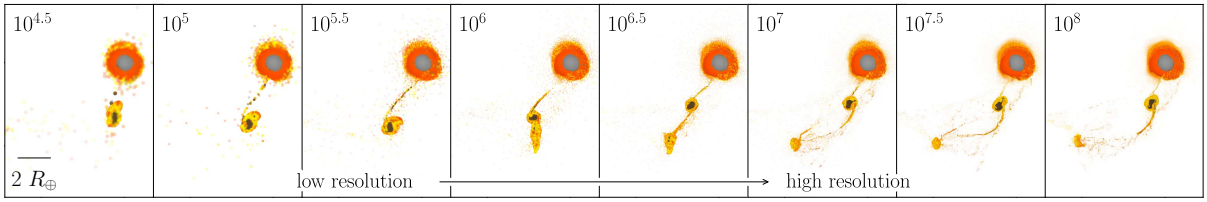

Figure 3: The categorically distinct behaviour of outer-satellite formation emerges consistently for resolutions above a threshold of $>10^{6.5}$ particles. Each panel shows a snapshot from simulations of the same scenario at the same time 3.6 h after impact using different numbers of particles.

Figure 4: An example render of a mid-impact snapshot from the second-animation simulation.

These data are read into Houdini and converted into particle geometries. Low-density particles with densities below 2500 kg m^{-3} are instead converted into voxel data, using the SPH smoothing kernel to compute the mass distribution. For a smoother animation, additional input snapshots are also created every 50 s by cubic-spline interpolation of the particle positions and properties.

The rendered colour, opacity, and emission of the particles and volumes are set by the SPH material, density, and specific internal energy (similar to the temperature). This allowed us to balance an accurate portrayal of the distribution and evolution of the material with minor aesthetic choices to help highlight points of dramatic and/or scientific interest; such as the stripping of bright, hot core material, or the form of the silicate atmosphere that surrounds the post-impact Earth without obscuring the orbiting or reimpacting debris. This development of the simulations and visualisations all within a single 'in-house' pipeline has also proved valuable for being able to control and update the rendering details and to apply and adapt the same techniques to other simulation projects.

Fig. 4 shows the resulting render for one example frame of the second animation. This linked video[5] shows a (somewhat arbitrary) selection of steps in the visualisation, sequentially adding to the render the: base particles; material colouring; directional lighting; iron light emission; low-density particles as volumes; mantle light emission; and minor compositing tweaks.

Additionally, a faint star map of the night sky was included as a background sphere. In reality, the brightness of the planets would far outshine any stars, but they are intended to subtly but intuitively help the viewer to understand the movement of the camera, since they give the eye reference points to, for example, distinguish between the planet spinning versus the camera tracking around.

4 Discussion

4.1 Scientific implications

By also running simulations at standard, lower resolutions, we find that the initial satellite separation is only consistent for simulations with over $10^{6.5}$

[5] icc.dur.ac.uk/giant_impacts/moon_houdini_steps.mp4

SPH particles, up to and including our highest resolution of 10^8, as shown in Fig. 3. Lower resolutions instead produce a single larger remnant that stays intact until it grazes or re-impacts the proto-Earth to produce a spray of debris. This emphasises how crucial convergence tests and higher resolutions are for numerical studies in this field, even for core results such as the primary outcomes of a giant impact, and demonstrates an alternative scenario for the origin of the Moon.

Furthermore, the outer layers of these directly formed satellites are molten over cooler interiors and are composed of around 60% proto-Earth material. This could alleviate the tension between the Moon's Earth-like isotopic composition and the different signature expected for the impactor, depending on the evolution of the lunar magma ocean (Charlier et al., 2018; Johnson et al., 2021), alongside other details such as the mixing of the Earth's outer mantle (Meier et al., 2014; Deng et al., 2019a).

Immediate formation also provides a hitherto overlooked range of initial conditions for the Moon's early evolution: with a wider and/or more eccentric or inclined orbit – outside the Roche radius and potentially also the evection and eviction resonances (Touma and Wisdom, 1998). We also find that this provides the novel option of a solid or only partially molten interior.

To determine whether these satellites can explain other properties of the Moon in addition to the mass and iron content, bespoke future studies are required to extrapolate the simulation outputs reliably to the present day – as remains an ongoing challenge for standard debris-accretion models as well (Lock et al., 2020; Canup et al., 2021).

With this in mind, some of the other possible implications besides the lunar isotopic composition include, for example, that the Moon's thin crust may not be consistent with the fully molten Moon expected from the accretion of hot debris in other models (Pritchard and Stevenson, 2000; Charlier et al., 2018; Johnson et al., 2021). A cohesive interior and non-circular orbit might also help to explain the lunar fossil figure, depending on the extent of tidal heating (Matsuyama et al., 2021). Or a satellite on a wide, significantly inclined orbit, which we also find can be produced by a misaligned pre-impact spin, could preserve its inclination to help to explain the Moon's tilted orbit (Ćuk et al., 2016; Tian and Wisdom, 2020).

4.2 Visualisations

Rendering SPH simulations of giant impacts in 3D is a valuable way to communicate the findings of numerical studies like this to the general public. In addition, for both experts and non-experts, this provides a unique and intuitive sense of the scale and violence of these key events in our planet's history and planet formation in general. Compared with standard 2D projections, these renders highlight how much the planets are distorted and reshaped, and can cleanly present more of the simulation content at once across different visual depths and material densities.

Separately, they also offer a new perspective for understanding the numerical simulations themselves and their limitations. For example, seeing the lack of perfect symmetry either side of the impact plane is an intuitive indicator of the noise introduced by the finite numbers of particles used to model the planets. Or, the extent of oscillation of the satellite highlights the lack of material strength in these (and most comparable) simulations, which could be a valuable goal for future studies to test.

5 Conclusions

We have presented 3D visualisations of high-resolution simulations that reveal how giant impacts can immediately place a satellite into a wide orbit with a Moon-like mass and iron content. The new options opened up for the initial lunar orbit and internal structure and the resulting outer layers rich in proto-Earth material could help to explain the isotopic composition of the Moon and other unsolved or debated lunar mysteries. Satellites that pass inside the Roche limit can predictably survive on new, higher-periapsis orbits. This extends the range of impact scenarios that can produce Moon-like satellites, and is also a relevant process to consider in other planetary systems. These animations that are more visually cinematic than standard 2D projections, while remaining directly based on the simulation data, aim to be useful both for public and expert engagement.

Acknowledgements

The work was in part supported by Science and Technology Facilities Council (STFC) grants ST/P000541/1 and ST/T000244/1, and used the DiRAC@Durham facility managed by the Institute for Computational Cosmology on behalf of the STFC DiRAC HPC Facility (www.dirac.ac.uk). This equipment was funded by BEIS via STFC capital grants ST/K00042X/1, ST/P002293/1, ST/R002371/1 and ST/S002502/1, Durham University and STFC operations grant ST/R000832/1. DiRAC is part of the National e-Infrastructure. The research in this paper made use of the SWIFT open-source simulation code (Schaller et al., 2018), version 0.9.0. J.A.K. acknowledges support from STFC grants ST/N001494/1 and ST/T002565/1 and a NASA Postdoctoral Program Fellowship.

S.R-B. is supported by STFC grant ST/P006744/1 and Durham University. V.R.E. and R.J.M. are supported by STFC grant ST/T000244/1. T.D.S. is supported by STFC grants ST/T506047/1 and ST/V506643/1. L.F.A.T. acknowledges support from NASA Emerging Worlds Program award 80NSSC18K0499.

References

Asphaug, E. *Annu. Rev. Earth Planet. Sci.*, 42: 551–578, 2014.

Balsara, D. S. *J. Comput. Phys.*, 121:357–372, 1995.

Benz, W., Slattery, W. L., and Cameron, A. G. W. *Icarus*, 71(1):30–45, 1987.

Borrow, J. et al. *Proc. 13th SPHERIC Intl. Wksh.*, pages 44–51, 2018.

Cameron, A. G. W. and Ward, W. R. In *LPSC*, vol 7, page 120, 1976.

Canup, R. M. *Science*, 338:1052, 2012.

Canup, R. M. and Asphaug, E. *Nature*, 412(6848): 708–712, 2001.

Canup, R. M. et al. *arXiv e-prints*, arXiv:2103.02045, 2021.

Charlier, B. et al. *Geochem. Cosmo. Acta*, 234: 50–69, 2018.

Citron, R. I., Manga, M., and Tan, E. *Earth Planet. Sci. Lett.*, 491:58–66, 2018.

Ćuk, M. and Stewart, S. T. *Science*, 338:1047, 2012.

Ćuk, M. et al. *Nature*, 539:402–406, 2016.

Dauphas, N. *Nature*, 541(7638):521–524, 2017.

Deng, H. et al. *Astrophys. J.*, 887(2):211, 2019a.

Deng, H. et al. *Astrophys. J.*, 870(2):127, 2019b.

Genda, H. et al. *Icarus*, 262:58–66, 2015.

Gingold, R. A. and Monaghan, J. J. *Mon. Not. R. Astron. Soc.*, 181:375–389, 1977.

Gonnet, P. *SIAM J Sci. Comput.*, 37(1):C95–C121, 2015.

Hartmann, W. K. and Davis, D. R. *Icarus*, 24(4): 504–515, 1975.

Hosono, N. et al. *Publ. Astron. Soc. Jpn.*, 69:26, 2017.

Hosono, N. et al. *Nature Geoscience*, 12(6):418–423, 2019.

Johansen, A. et al. *arXiv e-prints*, arXiv:2102.08611, 2021.

Johnson, T. E. et al. *Earth and Planetary Science Letters*, 556:116721, 2021.

Kegerreis, J. A. et al. *Mon. Not. R. Astron. Soc.*, 487(4):1536, 2019.

Lock, S. J. et al. *J. Geophys. Res. (Planets)*, 123: 910–951, 2018.

Lock, S. J. et al. *Space Sci. Rev.*, 216(6):109, 2020.

Lucy, L. B. *Astrophys. J.*, 82:1013–1024, 1977.

Mastrobuono-Battisti, A. and Perets, H. B. *ArXiv e-prints*, 2017.

Matsuyama, I., Trinh, A., and Keane, J. T. *Planet. Sci. J*, 2(6):232, 2021.

Meier, M. M. M., Reufer, A., and Wieler, R. *Icarus*, 242:316–328, 2014.

Melosh, H. J. *PTRSA*, 372(2024):20130168–20130168, 2014.

Pritchard, M. E. and Stevenson, D. J. *Thermal Aspects of a Lunar Origin by Giant Impact*, pages 179–196. 2000.

Reufer, A. et al. *Icarus*, 221:296–299, 2012.

Rufu, R. and Canup, R. M. *J. Geophys. Res. (Planets)*, 125(8):e06312, 2020.

Rufu, R., Aharonson, O., and Perets, H. B. *Nature Geoscience*, 10(2):89–94, 2017.

Ruiz-Bonilla, S. et al. *Mon. Not. R. Astron. Soc.*, 500(3):2861–2870, 2021.

Schaller, M. et al. Astrophysics Source Code Library, 2018.

Schiller, M., Bizzarro, M., and Fernandes, V. A. *Nature*, 555(7697):507–510, 2018.

Springel, V. *Mon. Not. R. Astron. Soc.*, 364:1105–1134, 2005.

Stewart, S. T. et al. *arXiv e-prints*, arXiv:1910.04687, 2019.

Tian, Z. and Wisdom, J. *Proc. Nat. Aca. Sci. USA*, 117(27):15460–15464, 2020.

Touma, J. and Wisdom, J. *Astrophys. J.*, 115(4): 1653–1663, 1998.